Exploring the Big Bang with Femtoscopy

MÁTÉ CSANÁD [ID]

Department of Atomic Physics, ELTE Eötvös Loránd University, Pázmány P. s. 1/a, 1117 Budapest 1117, Hungary
Email: csanad@elte.hu

Exploring the fundamental constituents of the matter around us and in the Universe, as well as their interactions, is among the premier goals of physics. Investigating ultrarelativistic collisions in particle accelerators has delivered answers to these questions many times in the past decades. In this article we focus on the research aimed at recreating the matter that filled the Universe in the first microsecond after the Big Bang – but this time in collisions of heavy ions. In particular, we discuss the technique called femtoscopy, which provides us with a tool to understand the space–time structure of particle creation in heavy-ion collisions. We use Lévy-stable distributions to investigate this structure and explore its dependence on particle momentum and collision energy.

Introduction

The strong interaction is the fundamental interaction of Nature responsible for the interactions of quarks and gluons, i.e., the constituents of protons and neutrons, as well as for most of the mass of the observable Universe. One important conjecture about the strong interaction is confinement: charges of the strong interaction, i.e., coloured objects (quarks and gluons) are only observable as part of colour-neutral composite particles, hadrons. Through a series of discoveries (Adams *et al.* 2005; Adcox *et al.* 2005; Back *et al.* 2005; Arsene *et al.* 2005), it turned out in the last decades that in ultrarelativistic collisions of heavy nuclei, the so-called strongly interacting Quark Gluon Plasma (sQGP) is created, which is governed by the strong interaction. This matter filled the Universe for the first microsecond of its existence.
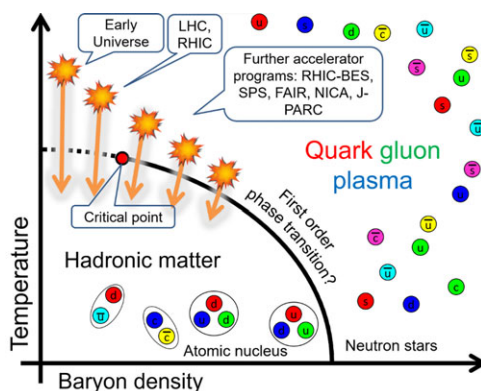
Figure 1. Phases of strongly interacting matter, as a function of temperature and baryon density. Arrows illustrate that lower-energy collider experiments probe the phase diagram at larger baryon densities and lower temperatures.

In this medium, coloured quarks and gluons, are independently interacting, i.e., confinement is lifted – this phenomenon is called deconfinement. At large collision energies, such as the ones available at the Relativistic Heavy Ion Collider (RHIC) or the Large Hadron Collider (LHC), the sQGP continuously transitions to form a hadronic matter, where colour is confined into colourless hadrons: baryons and mesons. This matter then expands, and particle detectors built around the collision point register its constituents. At lower collision energies, a first-order phase transition from deconfined to hadronic matter is expected, albeit not confirmed experimentally. At intermediate collision energy regions, a critical endpoint (CEP) of the phase diagram of the strongly interacting matter may be present. At this point, the transition between hadronic matter and the sQGP becomes a second-order phase transition. Figure 1 shows the phases of strongly interacting matter: at low baryon densities (quantifying the energy related to the baryon excess) and temperatures, hadronic matter is present, where quarks are confined into hadrons. At large densities or temperatures, colour may be deconfined, and the sQGP or other, exotic forms of matter (e.g., in neutron stars) may be present.

One of the most important goals of today's high-energy heavy ion physics is to confirm (or experimentally rule out) the existence of the CEP, and if it exists, to characterize its properties, e.g., the so-called critical exponents governing the rate of change of various thermodynamic quantities as a function of temperature. At various particle accelerator facilities, beam energy scan programmes were initiated to study this phase diagram. To do so, femtoscopic (momentum) correlations can be used to gain information about the femtometer-scale geometry of particle emission (Lednicky 2001). In this article, generalization of the conventional Gaussian analysis for the source geometry is discussed (Csörgő *et al.* 2004). Furthermore, recent measurements performed at various experiments are presented, as well as corresponding phenomenological interpretations that can be used to explore the phase diagram of strongly interacting matter.

The HBT Effect

Before going through the methodology of measuring and interpreting femtoscopic correlations in high-energy physics, let us mention that the origins of this field go back to R. Hanbury Brown and R. Q. Twiss, who investigated stars with optical and radio telescopes, at Jordell Bank and later at the Narrabri Observatory (Hanbury Brown *et al.* 1956). They discovered an unexplained correlation between signals of two telescopes, interpreted as coincidental photon detections happening 'too frequently' at the two telescopes, as compared with the expected frequency of random coincidences. They furthermore observed that this correlation (excess number of coincidences) decreases when increasing the distance between the two telescopes. Hanbury Brown later wrote in his autobiography:

> In fact, to a surprising number of people the idea that the arrival of photons at two separated detectors can ever be correlated was not only heretical but patently absurd, and they told us so in no uncertain terms, in person, by letter, in print, and by publishing the results of laboratory experiments, which claimed to show that we were wrong. (Hanbury Brown 1991)

Indeed, while these experiments were repeated in tabletop experiments as well, it took several decades to unravel the physics and mathematics behind this phenomenon, now called the HBT effect. There are two simple ways of understanding it. The first is (based on Baym 1998) to consider the optical or radio signal as spherical waves being emitted from a point *a* within the source, with the amplitude

$$A_a(r) = \frac{1}{|r - r_a|} \alpha e^{ik|r - r_a| + i\Phi_a}$$

where r is the spatial point at which we investigate the wave, r_a is the origin of the wave, α is its strength, k its wavenumber, and Φ_a is its phase, assumed to be a random variable with a uniform distribution in case of thermal emission. A similar amplitude can be expected from another point of the source; let us denote that one with a similar expression, but with index b and strength β. Let us assume that the source comprises only these two points, denoted by a and b. Then at any point in space, the wave amplitude from the source can be written as

$$A(r) = A_a(r) + A_b(r)$$

At the detectors, a sum of the waves emitted from both points of the source is detected. The observed intensity in detector A is then the square of the amplitude:

$$I_A = |A(r_A)|^2 = \frac{1}{L^2} \left(|\alpha|^2 + |\beta|^2 + \alpha^* \beta e^{ik(r_{bA} - r_{aA}) + i(\Phi_b - \Phi_a)} + c.c. \right)$$

where r_A is the location of detector A, L is the average distance between the source points and the detectors, while r_{bA} is the distance of source point b and detector A, similarly for r_{aA}, and *c.c.* denotes the complex conjugate of the preceding term.

The observed signal is then this intensity, averaged over a sufficiently large time interval, where phase information cancels out if the source is chaotic:

$$\langle I_A \rangle = \langle I_B \rangle = \frac{1}{L^2} \left(|\alpha|^2 + |\beta|^2 \right)$$

The joint (or coincident) intensity is, however, the product of intensities, where the phase information is retained even after averaging, resulting in an excess term as compared with the product of time-averaged intensities:

$$\langle I_A I_B \rangle = \langle I_A \rangle \langle I_B \rangle \left(1 + \frac{1}{2} \cos k (r_{aA} - r_{bA} + r_{aB} - r_{bB}) \right)$$

and

$$C_{AB} = \frac{\langle I_A I_B \rangle}{\langle I_A \rangle \langle I_B \rangle} \approx 1 + \frac{1}{2} \cos \frac{kRd}{L}$$

where the last approximation can be confirmed by expanding the sum of the distances in terms of d/L and R/L, where d is the distance of the detectors and R is the distance of the investigated source points. The factor $1/2$ in front of the cosine is specific to this configuration of two source points; the general result is the excess term, decreasing with increasing detector distance or source size. In a general source, an origin-dependent source strength $\alpha(r_s)$ would appear, and the sum would go over all possible r_s values; in fact, it would an integral instead of the $A_a(r) + A_b(r)$ sum written above.

A second way of understanding the HBT effect is when one considers the detection of two quantum-mechanical particles stemming from sources a and b, in detectors A and B. If we consider the two detection events separately, the corresponding wave functions are (assuming plane waves here for simplicity, but the calculation would work equivalently for spherical waves):

$$\Psi_B^b = e^{ikr_{bB} + i\Phi_b} \text{ and } \Psi_A^a = e^{ikr_{aA} + i\Phi_a}$$

If these particles are identical bosons (particles with integer intrinsic angular momentum, obeying Bose-Einstein statistics, e.g., photons), then the two-particle wave function must be symmetric with respect to particle exchange (cf. Bose–Einstein statistics), and the detection events are also entangled, expressible with the wave function

$$\Psi_{AB} = \frac{1}{\sqrt{2}} \left(\Psi_A^a \Psi_B^b + \Psi_B^a \Psi_A^b \right)$$

Then the single and joint detection probabilities are the modulus squares of the above wave functions for a single particle and the pair, respectively. In case of a setting similar to the one discussed in the classical derivation, the result in this case is:

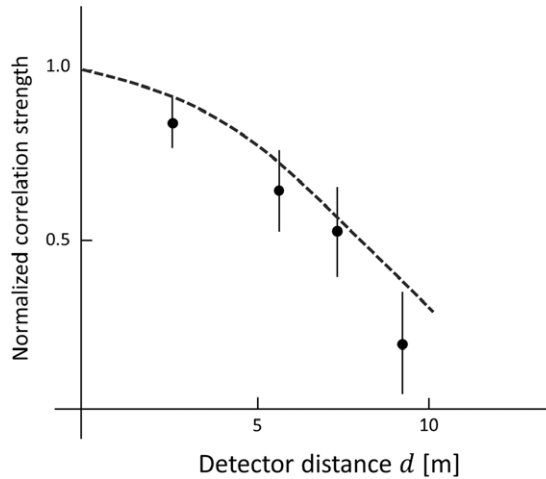$$C_{AB} = \frac{P(A,B)}{P(A)P(B)} = 1 + \cos k (r_{aA} - r_{bA} + r_{aB} - r_{bB}) \approx 1 + \cos k \frac{Rd}{L}$$

Figure 2. Correlation data from Sirius and a theoretical curve based on the calculation of a star of angular size 0.0063', reproduced from Hanbury Brown *et al.* (1956).

This second derivation can be extended to fermions (particles with half-odd-integer intrinsic angular momentum, obeying Fermi-Dirac statistics) as well, in which case a similar anti-correlation is observed. Furthermore, for an extended source, a source weight could appear as a prefactor in Ψ and an integral over r would have to be performed. Figure 2 shows example data from the measurement of Sirius by Hanbury Brown and Twiss, along with a calculation of such an extended source.

Femtoscopy

Independent of the HBT-discovery, Goldhaber and collaborators observed a similar correlation for pairs (Goldhaber *et al.* 1959) of pions (hadrons made up of one quark and one antiquark of the lightest kind), detected in high-energy proton–proton collisions. A clear understanding of the background of the two related phenomena is owed to articles by Glauber, Baym and others (Glauber 1963; Baym 1998). The main result, applicable today in high-energy physics, is that the two-particle momentum correlation function is connected to the particle creation probability density. This can be understood based on the connection of the single-particle momentum distribution $N_1(p)$ expressed as

$$N_1(p) = \int S(r,p)|\Psi_p(r)|^2 dr$$

where $S(r,p)$ is the particle creation probability density (also called single-particle source, or simply source) at the space-time point r and momentum p (in other words, the infinitesimal probability of creating a particle with momentum p in point r, which would be a sum of two Dirac delta distributions in the above two-source example), $\Psi_p(r)$ is the single-particle wave function of a particle with momentum p, and the

integral runs over the entire space-time. Similarly, the two-particle momentum distribution $N_2(p_1, p_2)$ can be expressed as

$$N_2(p_1, p_2) = \int S(r_1, p_1) S(r_2, p_2) |\Psi_{p_1, p_2}(r_1, r_2)|^2 dr_1 dr_2$$

where

$$\Psi_2(r_1, r_2) = \frac{1}{\sqrt{2}} \left(\Psi_{p_1}(r_1) \Psi_{p_2}(r_2) + \Psi_{p_2}(r_1) \Psi_{p_1}(r_2) \right)$$

is the two-particle symmetrized wave-function (for identical bosons). Assuming plane waves (i.e., neglecting interactions), defining $q = p_1 - p_2$, $K = (p_1 + p_2)/2$ and using the approximation that $q \ll K$, one obtains for the correlation function of identical bosons

$$C(q, K) = \frac{N_2(q + K, q - K)}{N_1(q + K) N_1(q - K)} \approx 1 + \frac{\left| \int dr S(r, K) e^{iqr} \right|^2}{\left| \int dr S(r, K) \right|^2} = 1 + \frac{|\tilde{S}(q, K)|^2}{|\tilde{S}(0, K)|^2}$$

where the tilde denotes the Fourier transform in the first variable. If one introduces the spatial correlation function as

$$D(r, K) = \int S\left(\rho + \frac{r}{2}, K\right) S\left(\rho - \frac{r}{2}, K\right) d\rho$$

and assumes it to be normalized to unity, then one obtains

$$C(q, K) = 1 + \int dr D(r, K) e^{iqr} = 1 + \tilde{D}(q, K)$$

The main result here is that the momentum correlation function is directly and simply connected to the spatial (pair) distribution. In femtoscopy, one often assumes a parametric shape for the r-dependence of S or D, and then the momentum dependence is expressible through the dependence of the parameters on K. For example, if the source is a Gaussian:

$$S(r, K) \sim \exp\left[-\frac{r^2}{2R(K)^2} \right]$$

or equivalently

$$D(r, K) \sim \exp\left[-\frac{r^2}{R(K)^2} \right]$$

then

$$C(q, K) = 1 + \exp\left[-q^2 R(K)^2 \right]$$

hence a source of some given width R creates correlations of inverse width $1/R$. This is illustrated by Figure 3; and this width is then also called the HBT radius (after the HBT effect).

This simple picture neglects several phenomena, such as final-state interactions (FSI), secondary particle production and multiparticle correlations. For details about these, see for example Adare *et al.* (2018) and Nagy *et al.* (2023). We only note here that in case of secondary particle production from decays of long-lived
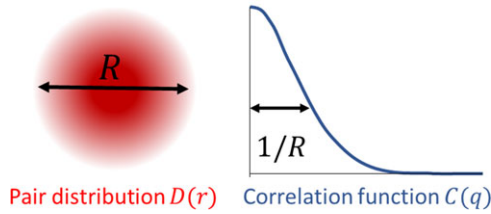
Figure 3. A source of width R creating correlations of width $1/R$.

resonances, the correlation strength decreases (Adare *et al.* 2018), and the correlation function (for the same Gaussian source as above) becomes

$$C(q, K) = 1 + \lambda(K) \cdot \exp\left[-q^2 R(K)^2\right]$$

where $\lambda(K)$ is the (momentum-dependent) correlation strength, which can be interpreted as the squared fraction of the primordially produced particles (Adare *et al.* 2018). Let us note at this point that, in experimental analyses, usually the dependence on $m_T = \sqrt{m^2 + K^2}$ (where m is the identified particle's mass) is investigated instead of the dependence on K.

Lévy-stable Sources

Due to the central limit theorem and thermodynamics leading to Gaussians, the natural assumption for the source shape is that of a Gaussian, and this assumption has been explored in a multitude of experimental and phenomenological investigations (Lisa *et al.* 2005). In this article we refrain from discussing those and instead focus on a different avenue of research. As mentioned in several references (Csörgő *et al.* 2004; Csanád *et al.* 2007 Adare *et al.* 2018), measurements (see, for example, Adler *et al.* 2007 or references in Adare *et al.* 2018) suggest phenomena beyond the Gaussian distribution. A straightforward generalization of the central-limit theorem for random variables without a finite variance or mean leads to a general class of distributions. Out of these we focus here on symmetric Lévy-stable distributions (Csörgő *et al.* 2004), defined as

$$\mathcal{L}(r; \alpha, R) = (2\pi)^{-3} \int dq e^{iqr} e^{-\frac{1}{2}|qR|^\alpha}$$

where r is the (three-dimensional) variable of the distribution, Lévy-index α and Lévy-scale R are its parameters, q is an integration variable, and qr is the scalar product of q and r. The distributions are stable for $0 < \alpha \leq 2$, meaning that a sum of random variables with such distribution converges to a random variable with the same distribution. In case of $\alpha < 2$ and three dimensions, these distributions exhibit a power law tail with exponent $-(1 + \alpha)$. For $\alpha = 2$, the Gaussian distribution is retained, while for $\alpha = 1$ one obtains the Cauchy (Lorentz) distribution. Note that the Lévy-scale R can also be called the HBT radius, but one has to keep in mind that
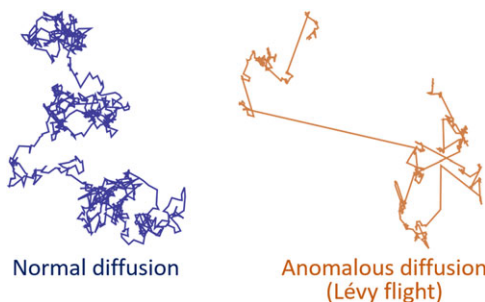
Figure 4. Examples for normal and anomalous diffusion in two dimensions. (Images modified from Wikipedia.)

it is conceptually a different observable from the one extracted from Gaussian measurements (except if α is close to 2).

If the single-particle source is of the Lévy-stable shape discussed above, then the pair source is also Lévy-stable with the same exponent, but modified width:

$$S(r) = \mathcal{L}(r; \alpha, R) \Rightarrow D(r) = \mathcal{L}\left(r; \alpha, 2^{1/\alpha}R\right)$$

where we dropped the dependence on mean momentum K for simplicity.

There may be several reasons for the appearance of these distributions, see a short review in Csanád *et al.* (2024). One example is anomalous diffusion (Csanád *et al.* 2007), as illustrated in Figure 4, where it is also apparent that in case of anomalous diffusion (also called Lévy flight) the appearance of large step sizes is much more frequent than in normal diffusion, creating a heavy tail in the resulting distribution.

Another example for the reasons of appearance of Lévy-stable distributions may be a second-order phase transition in the vicinity of the CEP, as detailed in Csörgő *et al.* (2006). It has been conjectured that at the critical point, the Lévy-exponent α introduced above is identical to the critical correlation exponent η, and hence drops to a much smaller value than 2, even down to values near 0.5 (Csörgő *et al.* 2006; Csanád *et al.* 2024).

Experimental Results and Interpretations

As detailed above, femtoscopy can be used to explore the probability density distribution of particle creation from the sQGP. The most abundant particles are pions; hence, their correlations can be measured most precisely (in terms of statistical uncertainty). The considerations in the previous section motivate the accurate measurement of the Lévy exponent α, but also measuring R with the correct source assumption is of crucial importance (Csanád *et al.* 2024). In this section we discuss several recent experimental results on these parameters.

The detailed centrality and average transverse mass dependence of these two-pion Lévy HBT parameters have been recently measured in 5.02 TeV Pb+Pb collisions
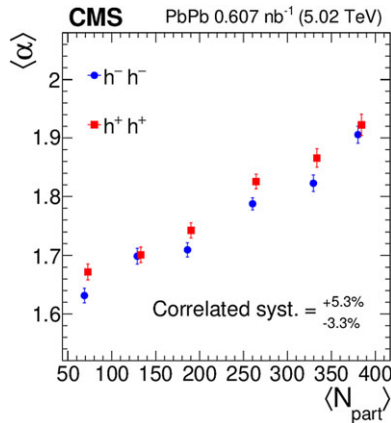
Figure 5. Lévy-index $\langle\alpha\rangle$ averaged over pair transverse mass, as a function of the number of participant nucleons (number of protons and nucleons involved in the collision, N_{part}), measured by CMS at LHC (figure reproduced from Tumasyan *et al.* 2024).

with the Compact Muon Solenoid (CMS) experiment at the LHC (Tumasyan *et al.* 2024). Here no particle identification was applied; instead, all detected particles were assumed to be pions. This reduces the correlation strength but does not change its shape, as non-pions do not contribute to the measured correlations. This analysis found qualitatively similar trends of the m_T-dependence of Lévy parameters as the first measurement of Lévy parameters in heavy-ion collisions, measured in 200 GeV Au+Au collisions by the Pioneering High Energy Nuclear Interaction eXperiment (PHENIX) at RHIC (Adare *et al.* 2018):

- a nearly constant $\alpha(m_T)$,
- a nearly constant $\lambda(m_T)$ at large m_T (when rescaled by the pion fraction),
- and an R decreasing with m_T as $R \propto \sqrt{m_T}$.

However, measured α values obtained by CMS were found to be around 1.6–2.0, significantly larger than those of PHENIX (where a mean value of $\alpha \approx 1.2$ was found in 0–30% Au+Au collisions). The α and R values measured by CMS are shown in Figures 5 and 6.

A similar analysis in the Solenoidal Tracker at RHIC (STAR) experiment was also performed in 200 GeV Au+Au collisions (Kincses 2024). Similar values, m_T-dependence, and centrality dependence for the Lévy index α, Lévy scale R and correlation strength λ were found as in Adare *et al.* (2018). Let us note in particular the decrease of $\lambda(m_T)$ at small m_T, attributed to a possible indirect signal of in-medium mass modification of the η' meson (Adare *et al.* 2018), a special particle made up of a quark and an antiquark from one of the three lightest kinds, with equal probability. The trends of the parameters versus m_T are also similar to the abovementioned CMS analysis (noting the difference in the accessible m_T interval); while the largest difference is that in the STAR measurement, α decreases for central collisions. Results by STAR on α and R are shown in Figures 7 and 8.
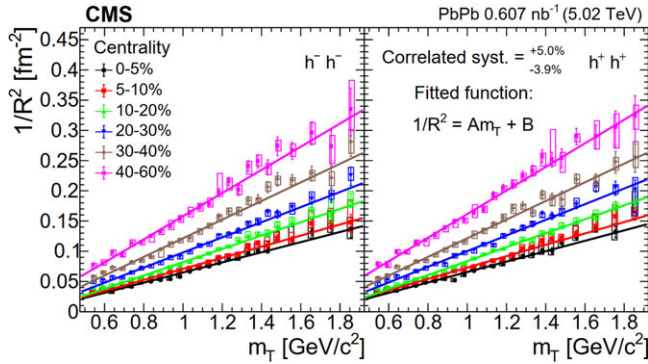
Figure 6. Lévy scale R as a function of pair transverse mass m_T, measured by CMS at LHC. Solid lines show linear fits based on hydrodynamic predictions (figure reproduced from Tumasyan 2024).
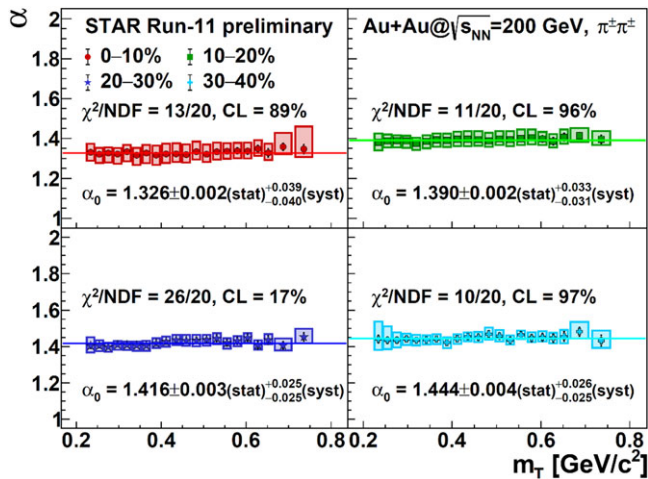

Figure 7. Lévy index α as a function of pair transverse mass m_T, measured by STAR at RHIC. Solid lines show constant fits (figure reproduced from Kincses 2024).

Measurements by the NA61/SHINE (SPS Heavy Ion and Neutrino Experiment) at the Super Proton Synchrotron (SPS) were reported for Be+Be collisions in Adhikary *et al.* (2023) and for Ar+Sc collisions in Pórfy (2024). These collision systems are initially significantly smaller than those in Au+Au collisions at RHIC and in Pb+Pb collisions at the LHC. The α values measured in Be+Be collisions were found to be around 1.6–2.0, similar to those obtained at the LHC. The ones measured in Ar+Sc collisions were found to be around 1.0–1.4, similar to those obtained at RHIC. The origin of this behaviour is as yet unexplained. The Lévy scale R shows a similar trend to the one at RHIC or LHC, but with smaller values, corresponding to the much smaller initial system size. Results from NA61/SHINE on
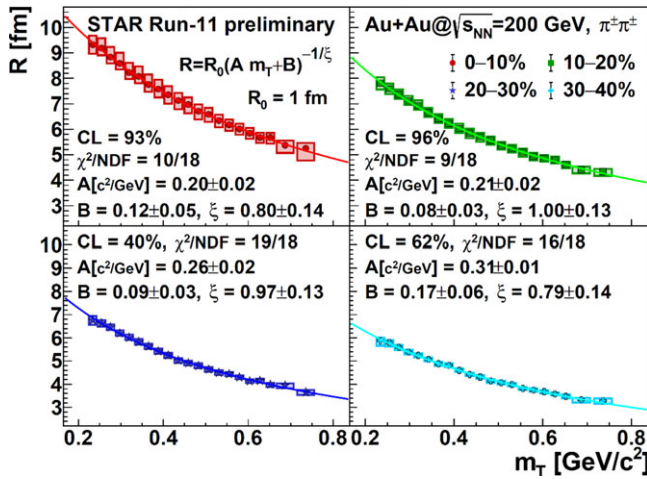
Figure 8. Lévy scale R as a function of pair transverse mass m_T, measured by STAR at RHIC. Solid lines show fits with an empirical curve (figure reproduced from Kincses 2024).
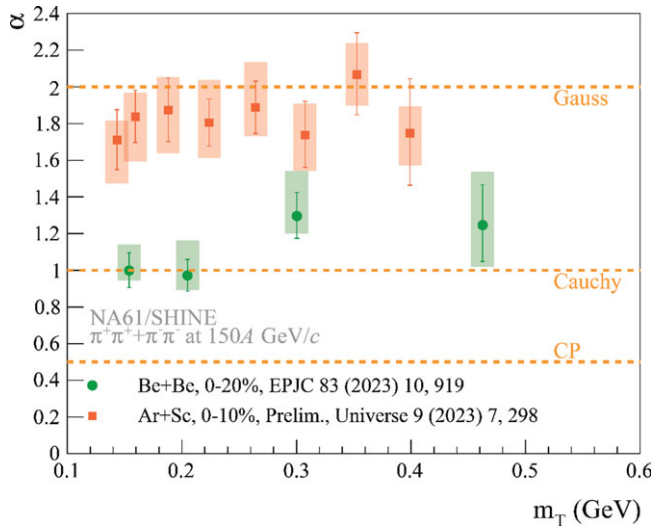

Figure 9. Lévy-index α as a function of pair transverse mass m_T, measured by NA61/ SHINE at SPS. Also shown are lines for special values of α (figure reproduced from Pórfy 2024).

α and R are shown in Figures 9 and 10. Note furthermore that the correlation strength λ does not show the characteristic decrease at small m_T observed at RHIC (and mentioned above). This hints at a difference in the physical processes occurring at SPS and at RHIC.
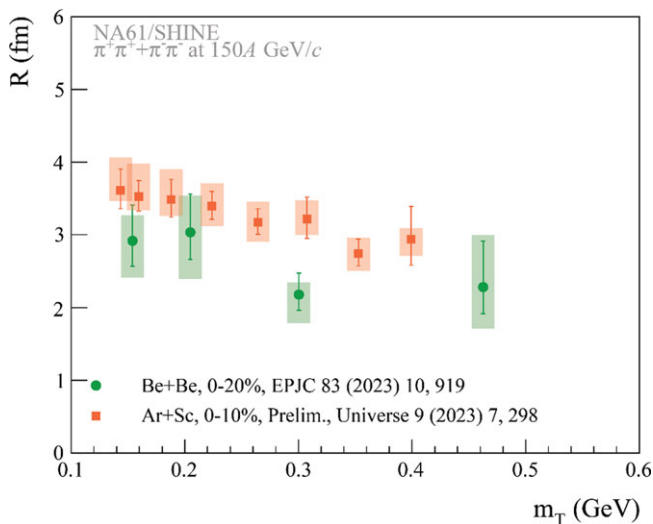
Figure 10. Lévy scale R as a function of pair transverse mass m_T, measured by NA61/SHINE at SPS (figure reproduced from Pórfy 2024).

Summary

Several phenomenological and experimental results related to femtoscopy have been presented. It was found that Lévy sources are observed at a wide range of collision energies, at SPS, at RHIC, and at the LHC. Multiple physical phenomena may influence the appearance of these sources: two examples discussed above are anomalous diffusion and critical phenomena. At LHC energies, as well as at higher RHIC energies, only the first (anomalous diffusion) may influence experimental correlation functions, as no critical phenomena are expected in this collision energy range. At lower RHIC energies or at the SPS, these may play a role as well. Observations, on the other hand, show varying values of Lévy exponent α: they are around 1.6–2.0 in SPS Be+Be collisions and LHC Pb+Pb collisions, while α values around 1.0–1.4 are found in SPS Ar+Sc collisions and RHIC Au+Au collisions. Furthermore, the opposite centrality dependence of α was found at RHIC and at LHC. Hence, it is clear that not only the collision energy but also the system size may influence these trends, and further explorations are needed to unravel the physical phenomena determining the shape of the particle-emitting source. Altogether, the measured Lévy exponents indicate a source that is clearly not Gaussian (i.e., $\alpha < 2$), thus underlining the importance of using Lévy-distributed source shapes.

The Lévy scale R was also measured in Be+Be and Ar+Sc collisions at SPS, in Au+Au collisions at RHIC and in Pb+Pb collisions at the LHC. A characteristic dependence on the transverse mass m_T was found at every energy and centrality: R decreases with m_T, as predicted based on the expanding nature of the fireball from which hadrons are created at the freeze-out. This dependence calls for detailed calculations and simulations to understand its origin: traditional hydrodynamic

calculations used in deriving this relationship were based on a Gaussian assumption for the source shape.

Finally, the correlation strength λ was also measured in the abovementioned systems. At RHIC, a decrease at small m_T was found, as well as a saturation at larger m_T values. The accessible range at LHC allowed only for the confirmation of the second trend. On the other hand, at SPS the mentioned decrease seemed to be absent, a difference that is expected to be explored in greater detail in higher precision SPS data as well.

The findings outlined above emphasize the importance of incorporating Lévy-shaped sources in femtoscopic analyses of momentum correlations measured in ultra-relativistic collisions of nuclei. To unravel the physical processes influencing the qualitative and quantitative details behind these observations, further phenomenological studies are required.

Acknowledgements

References

Adams J, Aggarwal MM, Ahammed Z, Amonett J, Anderson BD, Arkhipkin D, *et al.* (2005) Experimental and theoretical challenges in the search for the quark–gluon plasma: The STAR Collaboration's critical assessment of the evidence from RHIC collisions. *Nuclear Physics A* **757**, 102.

Adare A, Aidala C, Ajitanand NN, Akiba Y, Akimoto R, Alexander J, *et al.* (2018) Lévy-stable two-pion Bose-Einstein correlations in sqrt(*sNN*) = 200 GeV Au++Au collisions. *Physics Review C* **97**(6), 064911.

Adcox K, Adler SS, Afanasiev S, Aidala C, Ajitanand NN, Akiba Y, *et al.* (2005) Formation of dense partonic matter in relativistic nucleus–nucleus collisions at RHIC: Experimental evaluation by the PHENIX Collaboration. *Nuclear Physics A* **757**, 184.

Adhikary H, Adrich P, Allison K K, Amin N, Andronov E V, Anticic T, *et al.* (2023) Two-pion femtoscopic correlations in Be+Be collisions at sqrt(*sNN*)=16.84 GeV measured by the NA61/SHINE at CERN. *European Physics Journal C* **83**(10), 919.

Adler SS, Afanasiev S, Aidala C, Ajitanand NN, Akiba Y, Alexander J, *et al.* (2007) Evidence for a long-range component in the pion emission source in Au + Au collisions at $s(NN)^{**}(1/2) = 200$-GeV. *Physics Review Letters* **98**, 132301.

Arsene I, Bearden IG, Beavis D, Besliu C, Budick B, Boggild H, *et al.* (2005) Quark–gluon plasma and color glass condensate at RHIC? The perspective from the BRAHMS experiment. *Nuclear Physics A* **757**, 1.

Back BB, Baker MD, Ballintijn M, Barton DS, Becker B, Betts RR, *et al.* (2005) The PHOBOS perspective on discoveries at RHIC. *Nuclear Physics A* **757**, 28.

Baym G (1998) The physics of Hanbury Brown-Twiss intensity interferometry: from stars to nuclear collisions. *Acta Physica Polonica* **B29**, 1839.

Csanád M, Csörgő T and Nagy MI (2007) Anomalous diffusion of pions at RHIC. *Brazilian Journal of Physics* **37**, 1002–1013.

Csanád M and Kincses D (2024) Femtoscopy with Lévy sources from SPS through RHIC to LHC. *Universe* **10**(2), 54.

Csörgő T, Hegyi S and Zajc WA (2004) Bose-Einstein correlations for Levy stable source distributions. *European Physics Journal C* **36**, 67.

Csörgő T, Hegyi S, Novák T and Zajc WA (2006) Bose-Einstein or HBT correlation signature of a second order QCD phase transition. *AIP Conference Proceedings 2006*, **828**, 525–532.

Glauber RJ (1963) Photon correlations. *Physics Review Letters* **10**, 84–86.

Goldhaber G, Fowler WB, Goldhaber S and Hoang TF (1959) Pion-pion correlations in antiproton annihilation events. *Physics Review Letters* **3**, 181.

Hanbury Brown R (1991) *Boffin: A Personal Story of the Early Days of Radar, Radio Astronomy and Quantum Optics*. Bristol: Adam Hilger.

Hanbury Brown R and Twiss RQ (1956) A Test of a new type of stellar interferometer on Sirius. *Nature* **178**, 1046–1048.

Kincses D (2024) Pion interferometry with Levy sources in sqrt(sNN)= 200 GeV Au+Au Collisions at STAR. arXiv:2401.11169.

Lednicky R (2001) Femtoscopy with unlike particles. In *International Workshop on the Physics of the Quark Gluon Plasma*. arXiv:nucl-th/0112011.

Lisa MA, Pratt S, Soltz R and Wiedemann U (2005) Femtoscopy in relativistic heavy ion collisions: two decades of progress. *Annual Review of Nuclear and Particle Science* **55**, 357.

Nagy M, Purzsa A, Csanád M and Kincses D (2023) A novel method for calculating Bose–Einstein correlation functions with Coulomb final-state interaction. *European Physics Journal C* **83**(11), 1015.

Pórfy B (2024) Femtoscopy analysis in small systems at NA61/SHINE. *EPJ Web of Conferences* **296**, 06004.

Tumasyan A (2024) Two-particle Bose-Einstein correlations and their Lévy parameters in PbPb collisions at sqrt(sNN) = 5.02 TeV. *Physics Review C* **109**, 024914.

About the Author

Máté Csanád started his university studies at the University of Innsbruck (Austria), and obtained a Physics MSc degree at the Eötvös University (Hungary) in 2004. He pursued his graduate studies at the Stony Brook University (NY, USA) and at the Eötvös University, where he gained a PhD in 2007. After several semesters spent at CERN and at the Brookhaven National Laboratory, he now works at Eötvös University, where he also habilitated in 2013. He obtained his DSc degree from the Hungarian Academy of Sciences in 2021, and has been a professor since then. His interests focus on high energy heavy ion physics, hydrodynamic modelling of the quark gluon plasma, quantum statistical correlations and the femtometer spacetime structure of quark matter. He leads the Hungarian participation in experiments at the Relativistic Heavy Ion Collider, and is also a member in CERN experiments. His main research interests include the understanding of spatiotemporal structures on the femtometer scale via femtoscopy, as well as analytical solutions of relativistic hydrodynamics to understand the time evolution of matter created in collider experiments.